IOP Publishing Classical and Quantum Gravity

Class. Quantum Grav. **35** (2018) 065009 (25pp) https://doi.org/10.1088/1361-6382/aaab76

All-sky search for long-duration gravitational wave transients in the first Advanced LIGO observing run

B P Abbott[1], R Abbott[1], T D Abbott[2], M R Abernathy[3], F Acernese[4,5], K Ackley[6], C Adams[7], T Adams[8], P Addesso[9,144], R X Adhikari[1], V B Adya[10], C Affeldt[10], M Agathos[11], K Agatsuma[11], N Aggarwal[12], O D Aguiar[13], L Aiello[14,15], A Ain[16], P Ajith[17], B Allen[10,18,19], A Allocca[20,21], P A Altin[22], A Ananyeva[1], S B Anderson[1], W G Anderson[18], S Appert[1], K Arai[1], M C Araya[1], J S Areeda[23], N Arnaud[24], K G Arun[25], S Ascenzi[15,26], G Ashton[10], M Ast[27], S M Aston[7], P Astone[28], P Aufmuth[19], C Aulbert[10], A Avila-Alvarez[23], S Babak[29], P Bacon[30], M K M Bader[11], P T Baker[31,32], F Baldaccini[33,34], G Ballardin[35], S W Ballmer[36], J C Barayoga[1], S E Barclay[37], B C Barish[1], D Barker[38], F Barone[4,5], B Barr[37], L Barsotti[12], M Barsuglia[30], D Barta[39], J Bartlett[38], I Bartos[40], R Bassiri[41], A Basti[20,21], J C Batch[38], C Baune[10], V Bavigadda[35], M Bazzan[42,43], C Beer[10], M Bejger[44], I Belahcene[24], M Belgin[45], A S Bell[37], B K Berger[1], G Bergmann[10], C P L Berry[46], D Bersanetti[47,48], A Bertolini[11], J Betzwieser[7], S Bhagwat[36], R Bhandare[49], I A Bilenko[50], G Billingsley[1], C R Billman[6], J Birch[7], R Birney[51], O Birnholtz[10], S Biscans[1,12], A Bisht[19], M Bitossi[35], C Biwer[36], M A Bizouard[24], J K Blackburn[1], J Blackman[52], C D Blair[53], D G Blair[53], R M Blair[38], S Bloemen[54], O Bock[10], M Boer[55], G Bogaert[55], A Bohe[29], F Bondu[56], R Bonnand[8], B A Boom[11], R Bork[1], V Boschi[20,21], S Bose[57,16], Y Bouffanais[30], A Bozzi[35], C Bradaschia[21], P R Brady[18], V B Braginsky[50,145], M Branchesi[58,59], J E Brau[60], T Briant[61], A Brillet[55], M Brinkmann[10], V Brisson[24], P Brockill[18], J E Broida[62], A F Brooks[1], D A Brown[36], D D Brown[46], N M Brown[12], S Brunett[1], C C Buchanan[2], A Buikema[12], T Bulik[63], H J Bulten[64,11], A Buonanno[29,65], D Buskulic[8], C Buy[30], R L Byer[41], M Cabero[10], L Cadonati[45], G Cagnoli[66,67], C Cahillane[1], J Calderón Bustillo[45], T A Callister[1], E Calloni[5,68], J B Camp[69], M Canepa[47,48],

[145] Deceased, March 2016.

K C Cannon[70], H Cao[71], J Cao[72], C D Capano[10], E Capocasa[30], F Carbognani[35], S Caride[73], J Casanueva Diaz[24], C Casentini[15,26], S Caudill[18], M Cavaglià[74], F Cavalier[24], R Cavalieri[35], G Cella[21], C B Cepeda[1], L Cerboni Baiardi[58,59], G Cerretani[20,21], E Cesarini[15,26], S J Chamberlin[75], M Chan[37], S Chao[76], P Charlton[77], E Chassande-Mottin[30], B D Cheeseboro[31,32], H Y Chen[78], Y Chen[52], H-P Cheng[6], A Chincarini[48], A Chiummo[35], T Chmiel[79], H S Cho[80], M Cho[65], J H Chow[22], N Christensen[62], Q Chu[53], A J K Chua[81], S Chua[61], S Chung[53], G Ciani[6], F Clara[38], J A Clark[45], F Cleva[55], C Cocchieri[74], E Coccia[14,15], P-F Cohadon[61], A Colla[28,82], C G Collette[83], L Cominsky[84], M Constancio Jr.[13], L Conti[43], S J Cooper[46], T R Corbitt[2], N Cornish[85], A Corsi[73], S Cortese[35], C A Costa[13], M W Coughlin[62], S B Coughlin[86], J-P Coulon[55], S T Countryman[40], P Couvares[1], P B Covas[87], E E Cowan[45], D M Coward[53], M J Cowart[7], D C Coyne[1], R Coyne[73], J D E Creighton[18], T D Creighton[88], J Cripe[2], S G Crowder[89], T J Cullen[23], A Cumming[37], L Cunningham[37], E Cuoco[35], T Dal Canton[69], S L Danilishin[37], S D'Antonio[15], K Danzmann[10,19], A Dasgupta[90], C F Da Silva Costa[6], V Dattilo[35], I Dave[49], M Davier[24], G S Davies[37], D Davis[36], E J Daw[91], B Day[45], R Day[35], S De[36], D DeBra[41], G Debreczeni[39], J Degallaix[66], M De Laurentis[5,68], S Deléglise[61], W Del Pozzo[46], T Denker[10], T Dent[10], V Dergachev[29], R De Rosa[5,68], R T DeRosa[7], R DeSalvo[92], R C Devine[31,32], S Dhurandhar[16], M C Díaz[88], L Di Fiore[5], M Di Giovanni[93,94], T Di Girolamo[5,68], A Di Lieto[20,21], S Di Pace[28,82], I Di Palma[28,29,82], A Di Virgilio[21], Z Doctor[78], V Dolique[66], F Donovan[12], K L Dooley[74], S Doravari[10], I Dorrington[95], R Douglas[37], M Dovale Álvarez[46], T P Downes[18], M Drago[10], R W P Drever[1], J C Driggers[38], Z Du[72], M Ducrot[8], S E Dwyer[38], T B Edo[91], M C Edwards[62], A Effler[7], H-B Eggenstein[10], P Ehrens[1], J Eichholz[1], S S Eikenberry[6], R A Eisenstein[12], R C Essick[12], Z Etienne[31,32], T Etzel[1], M Evans[12], T M Evans[7], R Everett[75], M Factourovich[40], V Fafone[26,15,14], H Fair[36], S Fairhurst[95], X Fan[72], S Farinon[48], B Farr[78], W M Farr[46], E J Fauchon-Jones[95], M Favata[96], M Fays[95], H Fehrmann[10], M M Fejer[41], A Fernández Galiana[12], I Ferrante[20,21], E C Ferreira[13], F Ferrini[35], F Fidecaro[20,21], I Fiori[35], D Fiorucci[30], R P Fisher[36], R Flaminio[66,97], M Fletcher[37], H Fong[98], S S Forsyth[45], J-D Fournier[55], S Frasca[28,82], F Frasconi[21], Z Frei[99], A Freise[46], R Frey[60], V Frey[24], E M Fries[1], P Fritschel[12], V V Frolov[7], P Fulda[6,69], M Fyffe[7],

H Gabbard[10], B U Gadre[16], S M Gaebel[46], J R Gair[100], L Gammaitoni[33], S G Gaonkar[16], F Garufi[5,68], G Gaur[101], V Gayathri[102], N Gehrels[69], G Gemme[48], E Genin[35], A Gennai[21], J George[49], L Gergely[103], V Germain[8], S Ghonge[17], Abhirup Ghosh[17], Archisman Ghosh[11,17], S Ghosh[11,54], J A Giaime[2,7], K D Giardina[7], A Giazotto[21], K Gill[104], A Glaefke[37], E Goetz[10], R Goetz[6], L Gondan[99], G González[2], J M Gonzalez Castro[20,21], A Gopakumar[105], M L Gorodetsky[50], S E Gossan[1], M Gosselin[35], R Gouaty[8], A Grado[5,106], C Graef[37], M Granata[66], A Grant[37], S Gras[12], C Gray[38], G Greco[58,59], A C Green[46], P Groot[54], H Grote[10], S Grunewald[29], G M Guidi[58,59], X Guo[72], A Gupta[16], M K Gupta[90], K E Gushwa[1], E K Gustafson[1], R Gustafson[107], J J Hacker[23], B R Hall[57], E D Hall[1], G Hammond[37], M Haney[105], M M Hanke[10], J Hanks[38], C Hanna[75], J Hanson[7], T Hardwick[2], J Harms[58,59], G M Harry[3], I W Harry[29], M J Hart[37], M T Hartman[6], C-J Haster[46,98], K Haughian[37], J Healy[108], A Heidmann[61], M C Heintze[7], H Heitmann[55], P Hello[24], G Hemming[35], M Hendry[37], I S Heng[37], J Hennig[37], J Henry[108], A W Heptonstall[1], M Heurs[10,19], S Hild[37], D Hoak[35], D Hofman[66], K Holt[7], D E Holz[78], P Hopkins[95], J Hough[37], E A Houston[37], E J Howell[53], Y M Hu[10], E A Huerta[109], D Huet[24], B Hughey[104], S Husa[87], S H Huttner[37], T Huynh-Dinh[7], N Indik[10], D R Ingram[38], R Inta[73], H N Isa[37], J-M Isac[61], M Isi[1], T Isogai[12], B R Iyer[17], K Izumi[38], T Jacqmin[61], K Jani[45], P Jaranowski[110], S Jawahar[111], F Jiménez-Forteza[87], W W Johnson[2], D I Jones[112], R Jones[37], R J G Jonker[11], L Ju[53], J Junker[10], C V Kalaghatgi[95], V Kalogera[86], S Kandhasamy[74], G Kang[80], J B Kanner[1], S Karki[60], K S Karvinen[10], M Kasprzack[2], E Katsavounidis[12], W Katzman[7], S Kaufer[19], T Kaur[53], K Kawabe[38], F Kéfélian[55], D Keitel[87], D B Kelley[36], R Kennedy[91], J S Key[113], F Y Khalili[50], I Khan[14], S Khan[95], Z Khan[90], E A Khazanov[114], N Kijbunchoo[38], Chunglee Kim[115], J C Kim[116], Whansun Kim[117], W Kim[71], Y-M Kim[115,118], S J Kimbrell[45], E J King[71], P J King[38], R Kirchhoff[10], J S Kissel[38], B Klein[86], L Kleybolte[27], S Klimenko[6], P Koch[10], S M Koehlenbeck[10], S Koley[11], V Kondrashov[1], A Kontos[12], M Korobko[27], W Z Korth[1], I Kowalska[63], D B Kozak[1], C Krämer[10], V Kringel[10], B Krishnan[10], A Królak[119,120], G Kuehn[10], P Kumar[98], R Kumar[90], L Kuo[76], A Kutynia[119], B D Lackey[29,36], M Landry[38], R N Lang[18], J Lange[108], B Lantz[41], R K Lanza[12], A Lartaux-Vollard[24], P D Lasky[121], M Laxen[7], A Lazzarini[1], C Lazzaro[43], P Leaci[82,28], S Leavey[37], E O Lebigot[30], C H Lee[118], H K Lee[122], H M Lee[115], K Lee[37], J Lehmann[10],

A Lenon[31,32], M Leonardi[93,94], J R Leong[10], N Leroy[24], N Letendre[8], Y Levin[121], T G F Li[123], A Libson[12], T B Littenberg[124], J Liu[53], N A Lockerbie[111], A L Lombardi[45], L T London[95], J E Lord[36], M Lorenzini[14,15], V Loriette[125], M Lormand[7], G Losurdo[21], J D Lough[10,19], G Lovelace[23], H Lück[10,19], A P Lundgren[10], R Lynch[12], Y Ma[52], S Macfoy[51], B Machenschalk[10], M MacInnis[12], D M Macleod[2], F Magaña-Sandoval[36], E Majorana[28], I Maksimovic[125], V Malvezzi[15,26], N Man[55], V Mandic[126], V Mangano[37], G L Mansell[22], M Manske[18], M Mantovani[35], F Marchesoni[34,127], F Marion[8], S Márka[40], Z Márka[40], A S Markosyan[41], E Maros[1], F Martelli[58,59], L Martellini[55], I W Martin[37], D V Martynov[12], K Mason[12], A Masserot[8], T J Massinger[1], M Masso-Reid[37], S Mastrogiovanni[28,82], F Matichard[1,12], L Matone[40], N Mavalvala[12], N Mazumder[57], R McCarthy[38], D E McClelland[22], S McCormick[7], C McGrath[18], S C McGuire[128], G McIntyre[1], J McIver[1], D J McManus[22], T McRae[22], S T McWilliams[31,32], D Meacher[55,75], G D Meadors[10,29], J Meidam[11], A Melatos[129], G Mendell[38], D Mendoza-Gandara[10], R A Mercer[18], E L Merilh[38], M Merzougui[55], S Meshkov[1], C Messenger[37], C Messick[75], R Metzdorff[61], P M Meyers[126], F Mezzani[28,82], H Miao[46], C Michel[66], H Middleton[46], E E Mikhailov[130], L Milano[5,68], A L Miller[6,28,82], A Miller[86], B B Miller[86], J Miller[12], M Millhouse[85], Y Minenkov[15], J Ming[29], S Mirshekari[131], C Mishra[17], S Mitra[16], V P Mitrofanov[50], G Mitselmakher[6], R Mittleman[12], A Moggi[21], M Mohan[35], S R P Mohapatra[12], M Montani[58,59], B C Moore[96], C J Moore[81], D Moraru[38], G Moreno[38], S R Morriss[88], B Mours[8], C M Mow-Lowry[46], G Mueller[6], A W Muir[95], Arunava Mukherjee[17], D Mukherjee[18], S Mukherjee[88], N Mukund[16], A Mullavey[7], J Munch[71], E A M Muniz[23], P G Murray[37], A Mytidis[6], K Napier[45], I Nardecchia[15,26], L Naticchioni[28,82], G Nelemans[11,54], T J N Nelson[7], M Neri[47,48], M Nery[10], A Neunzert[107], J M Newport[3], G Newton[37], T T Nguyen[22], A B Nielsen[10], S Nissanke[11,54], A Nitz[10], A Noack[10], F Nocera[35], D Nolting[7], M E N Normandin[88], L K Nuttall[36], J Oberling[38], E Ochsner[18], E Oelker[12], G H Ogin[132], J J Oh[117], S H Oh[117], F Ohme[10,95], M Oliver[87], P Oppermann[10], Richard J Oram[7], B O'Reilly[7], R O'Shaughnessy[108], D J Ottaway[71], H Overmier[7], B J Owen[73], A E Pace[75], J Page[124], A Pai[102], S A Pai[49], J R Palamos[60], O Palashov[114], C Palomba[28], A Pal-Singh[27], H Pan[76], C Pankow[86], F Pannarale[95], B C Pant[49], F Paoletti[21,35], A Paoli[35], M A Papa[18,10,29], H R Paris[41], W Parker[7], D Pascucci[37], A Pasqualetti[35], R Passaquieti[20,21],

D Passuello[21], B Patricelli[20,21], B L Pearlstone[37], M Pedraza[1], R Pedurand[66,133], L Pekowsky[36], A Pele[7], S Penn[134], C J Perez[38], A Perreca[1], L M Perri[86], H P Pfeiffer[98], M Phelps[37], O J Piccinni[28,82], M Pichot[55], F Piergiovanni[58,59], V Pierro[9,144], G Pillant[35], L Pinard[66], I M Pinto[9,144], M Pitkin[37], M Poe[18], R Poggiani[20,21], P Popolizio[35], A Post[10], J Powell[37], J Prasad[16], J W W Pratt[104], V Predoi[95], T Prestegard[18,126], M Prijatelj[10,35], M Principe[9,144], S Privitera[29], R Prix[10], G A Prodi[93,94], L G Prokhorov[50], O Puncken[10], M Punturo[34], P Puppo[28], M Pürrer[29], H Qi[18], J Qin[53], S Qiu[121], V Quetschke[88], E A Quintero[1], R Quitzow-James[60], F J Raab[38], D S Rabeling[22], H Radkins[38], P Raffai[99], S Raja[49], C Rajan[49], M Rakhmanov[88], P Rapagnani[28,82], V Raymond[29], M Razzano[20,21], V Re[26], J Read[23], T Regimbau[55], L Rei[48], S Reid[51], D H Reitze[1,6], H Rew[130], S D Reyes[36], E Rhoades[104], F Ricci[28,82], K Riles[107], M Rizzo[108], N A Robertson[1,37], R Robie[37], F Robinet[24], A Rocchi[15], L Rolland[8], J G Rollins[1], V J Roma[60], J D Romano[88], R Romano[4,5], J H Romie[7], D Rosińska[44,135], S Rowan[37], A Rüdiger[10], P Ruggi[35], K Ryan[38], S Sachdev[1], T Sadecki[38], L Sadeghian[18], M Sakellariadou[136], L Salconi[35], M Saleem[102], F Salemi[10], A Samajdar[137], L Sammut[121], L M Sampson[86], E J Sanchez[1], V Sandberg[38], J R Sanders[36], B Sassolas[66], P R Saulson[36], O Sauter[107], R L Savage[38], A Sawadsky[19], P Schale[60], J Scheuer[86], E Schmidt[104], J Schmidt[10], P Schmidt[1,52], R Schnabel[27], R M S Schofield[60], A Schönbeck[27], E Schreiber[10], D Schuette[10,19], B F Schutz[29,95], S G Schwalbe[104], J Scott[37], S M Scott[22], D Sellers[7], A S Sengupta[138], D Sentenac[35], V Sequino[15,26], A Sergeev[114], Y Setyawati[11,54], D A Shaddock[22], T J Shaffer[38], M S Shahriar[86], B Shapiro[41], P Shawhan[65], A Sheperd[18], D H Shoemaker[12], D M Shoemaker[45], K Siellez[45], X Siemens[18], M Sieniawska[44], D Sigg[38], A D Silva[13], A Singer[1], L P Singer[69], A Singh[10,19,29], R Singh[2], A Singhal[14], A M Sintes[87], B J J Slagmolen[22], B Smith[7], J R Smith[23], R J E Smith[1], E J Son[117], B Sorazu[37], F Sorrentino[48], T Souradeep[16], A P Spencer[37], A K Srivastava[90], A Staley[40], M Steinke[10], J Steinlechner[37], S Steinlechner[27,37], D Steinmeyer[10,19], B C Stephens[18], S P Stevenson[46], R Stone[88], K A Strain[37], N Straniero[66], G Stratta[58,59], S E Strigin[50], R Sturani[131], A L Stuver[7], T Z Summerscales[139], L Sun[129], S Sunil[90], P J Sutton[95], B L Swinkels[35], M J Szczepańczyk[104], M Tacca[30], D Talukder[60], D B Tanner[6], M Tápai[103], A Taracchini[29], R Taylor[1], T Theeg[10], E G Thomas[46], M Thomas[7], P Thomas[38], K A Thorne[7],

E Thrane[121], T Tippens[45], S Tiwari[14,94], V Tiwari[95], K V Tokmakov[111], K Toland[37], C Tomlinson[91], M Tonelli[20,21], Z Tornasi[37], C I Torrie[1], D Töyrä[46], F Travasso[33,34], G Traylor[7], D Trifirò[74], J Trinastic[6], M C Tringali[93,94], L Trozzo[21,140], M Tse[12], R Tso[1], M Turconi[55], D Tuyenbayev[88], D Ugolini[141], C S Unnikrishnan[105], A L Urban[1], S A Usman[95], H Vahlbruch[19], G Vajente[1], G Valdes[88], N van Bakel[11], M van Beuzekom[11], J F J van den Brand[11,64], C Van Den Broeck[11], D C Vander-Hyde[36], L van der Schaaf[11], J V van Heijningen[11], A A van Veggel[37], M Vardaro[42,43], V Varma[52], S Vass[1], M Vasúth[39], A Vecchio[46], G Vedovato[43], J Veitch[46], P J Veitch[71], K Venkateswara[142], G Venugopalan[1], D Verkindt[8], F Vetrano[58,59], A Viceré[58,59], A D Viets[18], S Vinciguerra[46], D J Vine[51], J-Y Vinet[55], S Vitale[12], T Vo[36], H Vocca[33,34], C Vorvick[38], D V Voss[6], W D Vousden[46], S P Vyatchanin[50], A R Wade[1], L E Wade[79], M Wade[79], M Walker[2], L Wallace[1], S Walsh[10,29], G Wang[14,59], H Wang[46], M Wang[46], Y Wang[53], R L Ward[22], J Warner[38], M Was[8], J Watchi[83], B Weaver[38], L-W Wei[55], M Weinert[10], A J Weinstein[1], R Weiss[12], L Wen[53], P Weßels[10], T Westphal[10], K Wette[10], J T Whelan[108], B F Whiting[6], C Whittle[121], D Williams[37], R D Williams[1], A R Williamson[95], J L Willis[143], B Willke[10,19], M H Wimmer[10,19], W Winkler[10], C C Wipf[1], H Wittel[10,19], G Woan[37], J Woehler[10], J Worden[38], J L Wright[37], D S Wu[10], G Wu[7], W Yam[12], H Yamamoto[1], C C Yancey[65], M J Yap[22], Hang Yu[12], Haocun Yu[12], M Yvert[8], A Zadrożny[119], L Zangrando[43], M Zanolin[104], J-P Zendri[43], M Zevin[86], L Zhang[1], M Zhang[130], T Zhang[37], Y Zhang[108], C Zhao[53], M Zhou[86], Z Zhou[86], S J Zhu[10,29], X J Zhu[53], M E Zucker[1,12], J Zweizig[1] and LIGO Scientific Collaboration and Virgo Collaboration

[1] LIGO, California Institute of Technology, Pasadena, CA 91125, United States of America
[2] Louisiana State University, Baton Rouge, LA 70803, United States of America
[3] American University, Washington, D.C. 20016, United States of America
[4] Università di Salerno, Fisciano, I-84084 Salerno, Italy
[5] INFN, Sezione di Napoli, Complesso Universitario di Monte S.Angelo, I-80126 Napoli, Italy
[6] University of Florida, Gainesville, FL 32611, United States of America
[7] LIGO Livingston Observatory, Livingston, LA 70754, United States of America
[8] Laboratoire d'Annecy-le-Vieux de Physique des Particules (LAPP), Université Savoie Mont Blanc, CNRS/IN2P3, F-74941 Annecy-le-Vieux, France
[9] University of Sannio at Benevento, I-82100 Benevento, Italy
[10] Albert-Einstein-Institut, Max-Planck-Institut für Gravitationsphysik, D-30167 Hannover, Germany
[11] Nikhef, Science Park, 1098 XG Amsterdam, Netherlands

[12] LIGO, Massachusetts Institute of Technology, Cambridge, MA 02139, United States of America
[13] Instituto Nacional de Pesquisas Espaciais, 12227-010 São José dos Campos, São Paulo, Brazil
[14] INFN, Gran Sasso Science Institute, I-67100 L'Aquila, Italy
[15] INFN, Sezione di Roma Tor Vergata, I-00133 Roma, Italy
[16] Inter-University Centre for Astronomy and Astrophysics, Pune 411007, India
[17] International Centre for Theoretical Sciences, Tata Institute of Fundamental Research, Bengaluru 560089, India
[18] University of Wisconsin-Milwaukee, Milwaukee, WI 53201, United States of America
[19] Leibniz Universität Hannover, D-30167 Hannover, Germany
[20] Università di Pisa, I-56127 Pisa, Italy
[21] INFN, Sezione di Pisa, I-56127 Pisa, Italy
[22] Australian National University, Canberra, Australian Capital Territory 0200, Australia
[23] California State University Fullerton, Fullerton, CA 92831, United States of America
[24] LAL, University Paris-Sud, CNRS/IN2P3, Université Paris-Saclay, F-91898 Orsay, France
[25] Chennai Mathematical Institute, Chennai 603103, India
[26] Università di Roma Tor Vergata, I-00133 Roma, Italy
[27] Universität Hamburg, D-22761 Hamburg, Germany
[28] INFN, Sezione di Roma, I-00185 Roma, Italy
[29] Albert-Einstein-Institut, Max-Planck-Institut für Gravitationsphysik, D-14476 Potsdam-Golm, Germany
[30] APC, AstroParticule et Cosmologie, Université Paris Diderot, CNRS/IN2P3, CEA/Irfu, Observatoire de Paris, Sorbonne Paris Cité, F-75205 Paris Cedex 13, France
[31] West Virginia University, Morgantown, WV 26506, United States of America
[32] Center for Gravitational Waves and Cosmology, West Virginia University, Morgantown, WV 26505, United States of America
[33] Università di Perugia, I-06123 Perugia, Italy
[34] INFN, Sezione di Perugia, I-06123 Perugia, Italy
[35] European Gravitational Observatory (EGO), I-56021 Cascina, Pisa, Italy
[36] Syracuse University, Syracuse, NY 13244, United States of America
[37] SUPA, University of Glasgow, Glasgow G12 8QQ, United Kingdom
[38] LIGO Hanford Observatory, Richland, WA 99352, United States of America
[39] Wigner RCP, RMKI, H-1121 Budapest, Konkoly Thege Miklós út 29-33, Hungary
[40] Columbia University, New York, NY 10027, United States of America
[41] Stanford University, Stanford, CA 94305, United States of America
[42] Dipartimento di Fisica e Astronomia, Università di Padova, I-35131 Padova, Italy
[43] INFN, Sezione di Padova, I-35131 Padova, Italy
[44] Nicolaus Copernicus Astronomical Center, Polish Academy of Sciences, 00-716, Warsaw, Poland
[45] Center for Relativistic Astrophysics and School of Physics, Georgia Institute of Technology, Atlanta, GA 30332, United States of America
[46] University of Birmingham, Birmingham B15 2TT, United Kingdom
[47] Università degli Studi di Genova, I-16146 Genova, Italy
[48] INFN, Sezione di Genova, I-16146 Genova, Italy
[49] RRCAT, Indore MP 452013, India
[50] Faculty of Physics, Lomonosov Moscow State University, Moscow 119991, Russia
[51] SUPA, University of the West of Scotland, Paisley PA1 2BE, United Kingdom
[52] Caltech CaRT, Pasadena, CA 91125, United States of America

[53] University of Western Australia, Crawley, Western Australia 6009, Australia
[54] Department of Astrophysics/IMAPP, Radboud University Nijmegen, PO Box 9010, 6500 GL Nijmegen, Netherlands
[55] Artemis, Université Côte d'Azur, CNRS, Observatoire Côte d'Azur, CS 34229, F-06304 Nice Cedex 4, France
[56] Institut de Physique de Rennes, CNRS, Université de Rennes 1, F-35042 Rennes, France
[57] Washington State University, Pullman, WA 99164, United States of America
[58] Università degli Studi di Urbino 'Carlo Bo', I-61029 Urbino, Italy
[59] INFN, Sezione di Firenze, I-50019 Sesto Fiorentino, Firenze, Italy
[60] University of Oregon, Eugene, OR 97403, United States of America
[61] Laboratoire Kastler Brossel, UPMC-Sorbonne Universités, CNRS, ENS-PSL Research University, Collège de France, F-75005 Paris, France
[62] Carleton College, Northfield, MN 55057, United States of America
[63] Astronomical Observatory Warsaw University, 00-478 Warsaw, Poland
[64] VU University Amsterdam, 1081 HV Amsterdam, Netherlands
[65] University of Maryland, College Park, MD 20742, United States of America
[66] Laboratoire des Matériaux Avancés (LMA), CNRS/IN2P3, F-69622 Villeurbanne, France
[67] Université Claude Bernard Lyon 1, F-69622 Villeurbanne, France
[68] Università di Napoli 'Federico II', Complesso Universitario di Monte S.Angelo, I-80126 Napoli, Italy
[69] NASA/Goddard Space Flight Center, Greenbelt, MD 20771, United States of America
[70] RESCEU, University of Tokyo, Tokyo, 113-0033, Japan
[71] University of Adelaide, Adelaide, South Australia 5005, Australia
[72] Tsinghua University, Beijing 100084, People's Republic of China
[73] Texas Tech University, Lubbock, TX 79409, United States of America
[74] The University of Mississippi, University, MS 38677, United States of America
[75] The Pennsylvania State University, University Park, PA 16802, United States of America
[76] National Tsing Hua University, Hsinchu City, 30013 Taiwan, People's Republic of China
[77] Charles Sturt University, Wagga Wagga, New South Wales 2678, Australia
[78] University of Chicago, Chicago, IL 60637, United States of America
[79] Kenyon College, Gambier, OH 43022, United States of America
[80] Korea Institute of Science and Technology Information, Daejeon 305-806, Republic of Korea
[81] University of Cambridge, Cambridge CB2 1TN, United Kingdom
[82] Università di Roma 'La Sapienza', I-00185 Roma, Italy
[83] Université Libre de Bruxelles, Brussels 1050, Belgium
[84] Sonoma State University, Rohnert Park, CA 94928, United States of America
[85] Montana State University, Bozeman, MT 59717, United States of America
[86] Center for Interdisciplinary Exploration & Research in Astrophysics (CIERA), Northwestern University, Evanston, IL 60208, United States of America
[87] Universitat de les Illes Balears, IAC3—IEEC, E-07122 Palma de Mallorca, Spain
[88] The University of Texas Rio Grande Valley, Brownsville, TX 78520, United States of America
[89] Bellevue College, Bellevue, WA 98007, United States of America
[90] Institute for Plasma Research, Bhat, Gandhinagar 382428, India
[91] The University of Sheffield, Sheffield S10 2TN, United Kingdom
[92] California State University, Los Angeles, 5154 State University Dr, Los Angeles, CA 90032, United States of America

[93] Dipartimento di Fisica, Università di Trento, I-38123 Povo, Trento, Italy
[94] INFN, Trento Institute for Fundamental Physics and Applications, I-38123 Povo, Trento, Italy
[95] Cardiff University, Cardiff CF24 3AA, United Kingdom
[96] Montclair State University, Montclair, NJ 07043, United States of America
[97] National Astronomical Observatory of Japan, 2-21-1 Osawa, Mitaka, Tokyo 181-8588, Japan
[98] Canadian Institute for Theoretical Astrophysics, University of Toronto, Toronto, Ontario M5S 3H8, Canada
[99] MTA Eötvös University, 'Lendulet' Astrophysics Research Group, Budapest 1117, Hungary
[100] School of Mathematics, University of Edinburgh, Edinburgh EH9 3FD, United Kingdom
[101] University and Institute of Advanced Research, Gandhinagar, Gujarat 382007, India
[102] IISER-TVM, CET Campus, Trivandrum Kerala 695016, India
[103] University of Szeged, Dóm tér 9, Szeged 6720, Hungary
[104] Embry-Riddle Aeronautical University, Prescott, AZ 86301, United States of America
[105] Tata Institute of Fundamental Research, Mumbai 400005, India
[106] INAF, Osservatorio Astronomico di Capodimonte, I-80131, Napoli, Italy
[107] University of Michigan, Ann Arbor, MI 48109, United States of America
[108] Rochester Institute of Technology, Rochester, NY 14623, United States of America
[109] NCSA, University of Illinois at Urbana-Champaign, Urbana, IL 61801, United States of America
[110] University of Białystok, 15-424 Białystok, Poland
[111] SUPA, University of Strathclyde, Glasgow G1 1XQ, United Kingdom
[112] University of Southampton, Southampton SO17 1BJ, United Kingdom
[113] University of Washington Bothell, 18115 Campus Way NE, Bothell, WA 98011, United States of America
[114] Institute of Applied Physics, Nizhny Novgorod, 603950, Russia
[115] Seoul National University, Seoul 151-742, Republic of Korea
[116] Inje University Gimhae, 621-749 South Gyeongsang, Republic of Korea
[117] National Institute for Mathematical Sciences, Daejeon 305-390, Republic of Korea
[118] Pusan National University, Busan 609-735, Republic of Korea
[119] NCBJ, 05-400 Świerk-Otwock, Poland
[120] Institute of Mathematics, Polish Academy of Sciences, 00656 Warsaw, Poland
[121] The School of Physics & Astronomy, Monash University, Clayton 3800, Victoria, Australia
[122] Hanyang University, Seoul 133-791, Republic of Korea
[123] The Chinese University of Hong Kong, Shatin, NT, Hong Kong
[124] University of Alabama in Huntsville, Huntsville, AL 35899, United States of America
[125] ESPCI, CNRS, F-75005 Paris, France
[126] University of Minnesota, Minneapolis, MN 55455, United States of America
[127] Dipartimento di Fisica, Università di Camerino, I-62032 Camerino, Italy
[128] Southern University and A&M College, Baton Rouge, LA 70813, United States of America
[129] The University of Melbourne, Parkville, Victoria 3010, Australia
[130] College of William and Mary, Williamsburg, VA 23187, United States of America
[131] Instituto de Fí sica Teórica, University Estadual Paulista/ICTP South American Institute for Fundamental Research, São Paulo SP 01140-070, Brazil

[132] Whitman College, 345 Boyer Avenue, Walla Walla, WA 99362 United States of America
[133] Université de Lyon, F-69361 Lyon, France
[134] Hobart and William Smith Colleges, Geneva, NY 14456, United States of America
[135] Janusz Gil Institute of Astronomy, University of Zielona Góra, 65-265 Zielona Góra, Poland
[136] King's College London, University of London, London WC2R 2LS, United Kingdom
[137] IISER-Kolkata, Mohanpur, West Bengal 741252, India
[138] Indian Institute of Technology, Gandhinagar Ahmedabad Gujarat 382424, India
[139] Andrews University, Berrien Springs, MI 49104, United States of America
[140] Università di Siena, I-53100 Siena, Italy
[141] Trinity University, San Antonio, TX 78212, United States of America
[142] University of Washington, Seattle, WA 98195, United States of America
[143] Abilene Christian University, Abilene, TX 79699, United States of America
[144] INFN, Sezione di Napoli, I-80100 Napoli, Italy

E-mail: lvc.publications@ligo.org

Received 18 November 2017, revised 25 January 2018
Accepted for publication 30 January 2018
Published 14 February 2018

Abstract

We present the results of a search for long-duration gravitational wave transients in the data of the LIGO Hanford and LIGO Livingston second generation detectors between September 2015 and January 2016, with a total observational time of 49 d. The search targets gravitational wave transients of 10–500 s duration in a frequency band of 24–2048 Hz, with minimal assumptions about the signal waveform, polarization, source direction, or time of occurrence. No significant events were observed. As a result we set 90% confidence upper limits on the rate of long-duration gravitational wave transients for different types of gravitational wave signals. We also show that the search is sensitive to sources in the Galaxy emitting at least $\sim 10^{-8}\ M_{\odot}c^2$ in gravitational waves.

Keywords: LIGO-Virgo, gravitational waves, long duration transient

(Some figures may appear in colour only in the online journal)

1. Introduction

The first observing runs of the Advanced LIGO and Advanced Virgo detectors, with significant sensitivity improvements compared to the first generation detectors, yielded in less than two years incredible discoveries and major astrophysics results via gravitational wave (GW) detections. The first observed GW signals corresponded to the final moments of the coalescence of two stellar-mass black holes and their final plunge. GW150914 and GW151226 were observed with high confidence ($>5\sigma$), while LVT151012 was identified with a lower significance (1.7σ) [1–5] during the first observing run (O1). During the second observing run (O2), GW170104 and GW170814 (which was detected simultaneously by the three LIGO and Virgo detectors) have confirmed the estimated rate of stellar-mass black hole mergers [6, 7]. Lastly,

the observation of a binary neutron star inspiral by the LIGO and Virgo network [8] in association with a gamma-ray burst [9] and a multitude of broadband electromagnetic counterpart observations [10] has opened up a new era in multimessenger astronomy.

The searches that observed these binary compact object systems were also targetting neutron star—black hole mergers [11, 12] as well as intermediate-mass black hole mergers of total mass up to 600 $M_\odot$ [13]. So far, only O1 observing run results have been reported for these sources, and no other compact binary coalescence, nor any short duration signal targeted by unmodeled short duration searches [12] have been observed.

In this paper, we present an all-sky search for unmodeled long-duration (10–500 s) transient GW events. Astrophysical compact sources undergoing complex dynamics and hydrodynamic instabilities are expected to emit long-lasting GWs. For example, fallback accretion onto a newborn neutron star can lead to a non-axisymmetric deformation which emits GWs until the neutron star collapses to a black hole [14–17]. Non-axisymmetric accretion disc fragmentation and instabilities can lead to material spiraling into the central stellar-mass black hole, emitting GWs [18–20]. Long-duration GWs may also be emitted by non-axisymmetric deformations in magnetars [21, 22], which are possible progenitors of long and short GRBs [23, 24]. Finally, core-collapse supernovae simulations have shown that the turbulent and chaotic fluid movements that occur in the proto-neutron star formed a few hundred milliseconds after the core collapse can excite long-lasting surface g-modes whose frequency drifts over time [25, 26].

We extend the search for long-duration GW transients previously carried out on initial LIGO data from the period 2005–2010 [27]. Four pipelines have been used to double the frequency band coverage from (40–1000 Hz) to (24–2048 Hz), and new waveform models have been used to estimate the pipelines' sensitivities. We explicitly demonstrate that the search is capable of efficiently detecting three of the four potential sources mentioned above. No significant events were detected and consequently, upper limits have been set on the rate of long-duration transient signals.

The organization of the paper is as follows. In section 2, we describe the dataset. Section 3 is devoted to a brief description of the pipelines, whose sensitivities are presented in section 4. In section 5, we give and discuss the results, then we conclude in section 6 with a discussion of future expectations.

2. Data set and data quality

This O1 analysis uses data from 12 September 2015 to 19 January 2016. The LIGO detectors in Hanford, WA and Livingston, LA ran with 40% coincident time. For this long-duration transient search, about two days of coincident data have been discarded because they were affected by major detector failures or problematic weather conditions. The remaining 49 d of coincident data still contain many non-stationary short duration noise events that can mimic a signal. These noise events, refered to as 'glitches', can last from a fraction of a second up to several seconds and have a multitude of causes. For instance, low frequency glitches are caused by surges in power lines or seismic events, while many high frequency glitches are caused by resonances in the test mass suspension wires [28]. Many of these effects can be tracked in auxiliary sensors that we use to define the severity of the loss of data quality [28–30].

The signals targeted by the long-duration transients search have their energy spread over a large time span. Consequently, even modest excesses of noise directly influence the signal reconstruction. In order to be considered as a potential real signal, events must be seen

coincidently in the two LIGO detectors. This requirement eliminates most of the noise events due to glitches. An accurate background estimation using the data themselves is therefore necessary to measure the significance of any coincident excess of energy. A false alarm rate (FAR) is estimated after safe veto methods are applied to get rid of as many glitch events as possible. While a few families of these noise events can be suppressed by vetoes based on auxiliary channels, each search pipeline has its own background reduction strategy and its own implementation of the time-slides method [31] to estimate the FAR. It consists in introducing a time-shift in one detector's strain time series. Details on these topics are provided in the next section.

3. Pipelines

Four pipelines are used to analyze the data set and search for long-duration GW transient signals. These pipelines are described in the sub-sections that follow.

3.1. Coherent waveburst

Coherent WaveBurst (cWB) is a pipeline designed to search for generic GW transients. Using a maximum-likelihood-ratio statistic [32], it identifies coincident excess power events (triggers) in a time-frequency space. The long-duration transient cWB search is implemented with the same pipeline also used to search for short transient events [12] with a few specific changes: It operates in the frequency range 24–2048 Hz and only data which pass the strictest data quality criteria are examined (see section 2 and [12]). Events are ranked according to their detection statistic (η_c), which is related to the event signal-to-noise ratio (SNR). A primary selection is based on the network correlation coefficient C_c [32], which measures the degree of correlation between the detectors, and the energy-weighted duration of detected triggers.

$$C_c = \frac{|E_c|}{|E_c| + E_n}, \tag{1}$$

E_c is the coherent energy and E_n is the null stream energy [32]. C_c is thus bounded between 0 and 1 and provides a powerful test to distinguish genuine GW events ($C_c \sim 1$) from spurious events ($C_c \ll 1$) produced by the detectors. Events with $C_c < 0.6$ or duration <1.5 s are excluded from the analysis. The selection criterion based on duration is specific to this long-duration search and it is the most powerful selection criteria to suppress background triggers. To characterize the FAR, the data of one interferometer is shifted in time (the so called time-slides method) with respect to the other interferometer by multiple delays of 1 s for an equivalent total time of $\sim$70 years of coincident time.

3.2. The STAMP-AS pipeline

The all-sky STAMP-AS pipeline based on the stochastic transient analysis multi-detector pipeline [27] cross-correlates data from two detectors and builds coherent time-frequency maps (*tf*-maps) of SNR with a pixel size of 1 s $\times$ 1 Hz. The SNR is computed for each second of data by estimating the mean noise over the neighboring seconds on each side. Pixels in frequency bins corresponding to known instrumental lines are suppressed. Once the *tf*-maps are built, overlapping clusters that pass a SNR threshold of 0.75 are grouped to form triggers. There are two variants of STAMP-AS that differ in cluster grouping strategy: Zebragard and Lonetrack.

3.2.1. Zebragard. Working with *tf*-maps of size 24–2000 Hz $\times$ 500 s, Zebragard groups together pixels above a given SNR threshold that lie within a 4 pixel distance from each other. Because a sub-optimal number of sky positions are targeted, a signal can be anti-coherent (negative SNR). The algorithm addresses this in such a way that the loss of efficiency due to the limited number of tested sky positions is less than 10% [33]. The trigger ranking statistic, Θ_Γ, is defined as the quadratic sum of the SNR of the individual pixels. This analysis uses the same configuration and the same background rejection strategy against short-duration noise transient 'glitches' (the fraction of SNR in each time bin must be smaller than 0.5) as in [27]. In addition, the O1 data set contains an excess of background triggers that required developing additional vetoes. For example, using the fact that the two LIGO detectors are almost aligned, triggers due to a loud glitch in one detector are suppressed by demanding that the SNR ratio between the two detectors is smaller than 3. Mechanical resonances excited when the optical cavities of the interferometer arms are locked generate an excess of triggers at 39 Hz and 43 Hz at well identified times. Finally, the remaining glitches are efficiently suppressed by data quality vetoes based on auxiliary channels [34]. It has been verified that these vetoes minimally affect the search for the targeted signals (less than 5% of simulated signals are lost). The background is estimated by time-shifting the data of one detector relative to the other in steps of 250 s. Data quality investigations and veto tuning are performed using a subset of the time-shifted triggers. The background rate is estimated with 600 time shift values between the detectors for an equivalent total time of $\sim$78 years of coincident time for the O1 data set.

3.2.2. Lonetrack. Lonetrack uses seedless clustering to integrate the signal power along spectrogram tracks using templates chosen to capture the salient features of a wide class of signal models. Templates here are not meant to exactly match the signal but rather to identify a few isolated pixels that are part of the signals. Bézier curves [35–39], a post-Newtonian expansion for time-frequency track of circular compact binary coalescence signals [40], and an analytic expression for low-to-moderate eccentric compact binaries [41] have all been used previously as seedless clustering parametrizations. These parameterizations are used to create template banks of frequency-time tracks. In this present search, Bézier curves were used in order to be sensitive to as many signal models as possible.

The Lonetrack search hierarchically selects the most promising triggers. This allows us to estimate the events' significance at very low FAR (to reach the equivalent of 5σ detection probability). It begins by applying seedless clustering to analyze spectrograms of a single-detector, incoherent statistic [39]. For times that pass a threshold on SNR of 6, *tf*-maps of cross-power SNR are constructed using the tracks derived from the single detector, incoherent statistic. This analysis is carried out for 400 evenly spaced values of 0.05 ms time delay between the detectors. The FAR is estimated with an equivalent total time of $\sim$12 000 years. The detection statistic to rank triggers is the maximum SNR found per map.

3.3. X-SphRad

The x-pipeline spherical radiometer (X-SphRad) is a fast cross-correlator in the spherical harmonic domain [42]. The spherical radiometry approach takes advantage of the fact that sky maps in GW searches show strong correlations over large angular scales in a pattern determined by the network geometry [43]. Computing sky maps indirectly through their spherical harmonics minimizes the number of redundant calculations, allowing the data to be processed independently of sky position. The pipeline is built on X-pipeline [44, 45] which whitens the data in the pre-processing step and then post-processes the event triggers output using the spherical radiometer. The pipeline uses the ratio of the power in the homogeneous polynomials

of degree $l > 0$ modes to that in the $l = 0$ mode to rank triggers. This ranking statistic provides a discriminatory power for rejecting background glitches [46]. To estimate the background, X-SphRad time-shifts the data for each detector in the network. The X-SphRad O1 search used an equivalent total time of 57 years and covers the frequency band 24–1000 Hz.

4. Sensitivity

The sensitivity of each pipeline is estimated using 22 different types of simulated GW signals. Half of these are based on astrophysical source models and can be divided into 3 families: fallback accretion onto neutron stars (FA), black hole accretion disk instabilities (ADI) and magnetars. The other waveforms have ad-hoc morphologies that encapsulate the main characteristics for long-duration transients. The next section briefly describes the models of sources whose chosen parameters are given in table 1. Figure 1 shows the spectrogram of some of the signal waveforms.

4.1. Waveform descriptions

FA: The fallback accretion disk model [17] focuses on newly born spinning neutron stars. In some unstable configurations, a non-axisymmetric deformation appears causing the production of GWs. The signal lasts from $\sim$10 s up to a few 100 s and its frequency evolution is almost linear.

ADI: This family includes five waveforms already considered and described in the LIGO S5/S6 search [27] and the O1 GRB search [47]. In this model [19, 20], a thick accretion disk is coupled to a Kerr black hole through strong magnetic fields. This coupling is thought to generate turbulence in the accretion torus that may form clumps of matter. The quadrupole components of the disk lead to gravitational wave emission that spin down the black hole and separate the clumps. The anti-chirp like waveform (frequency and amplitude decreases over time) depends on the mass of the central black hole M, the Kerr spin parameter a_*, and the fraction ϵ of the disk mass that forms clumps.

Magnetar: Magnetic deformation of a rapidly rotating neutron star can generate long-lasting GWs that can live up to one hour with a slowly decreasing frequency and amplitude (i.e. an anti-chirp). We used the model described in [48], which includes two parameters: the magnetic ellipticity ϵ_b and the spin frequency f_0 of the neutron star, that entirely describe the frequency and amplitude variations.

Ad-hoc waveforms: These include monochromatic waveforms (MONO) and waveforms with a linear (LINE) and quadratic (QUAD) frequency evolution, as well as white noise band-limited (WNB) and sine-Gaussian bursts (SG) [27]. All of these waveforms have duration from $\sim$10 s up to a few 100 s and frequencies spanning the analysis range.

4.2. Detection efficiencies

In order to determine the detection efficiencies, waveforms have been added coherently to the detector data at randomly chosen times over the full run period. We are using waveforms (H_+ and $H_\times$ polarizations) that have been generated in the frame of the source. For each chosen time we draw a source sky position such that the whole set of source positions is uniformly distributed over the sky. In the frame of the detector the waveforms are elliptically polarized with an ellipticity that varies uniformally between 0 and 1. The waveform amplitudes are

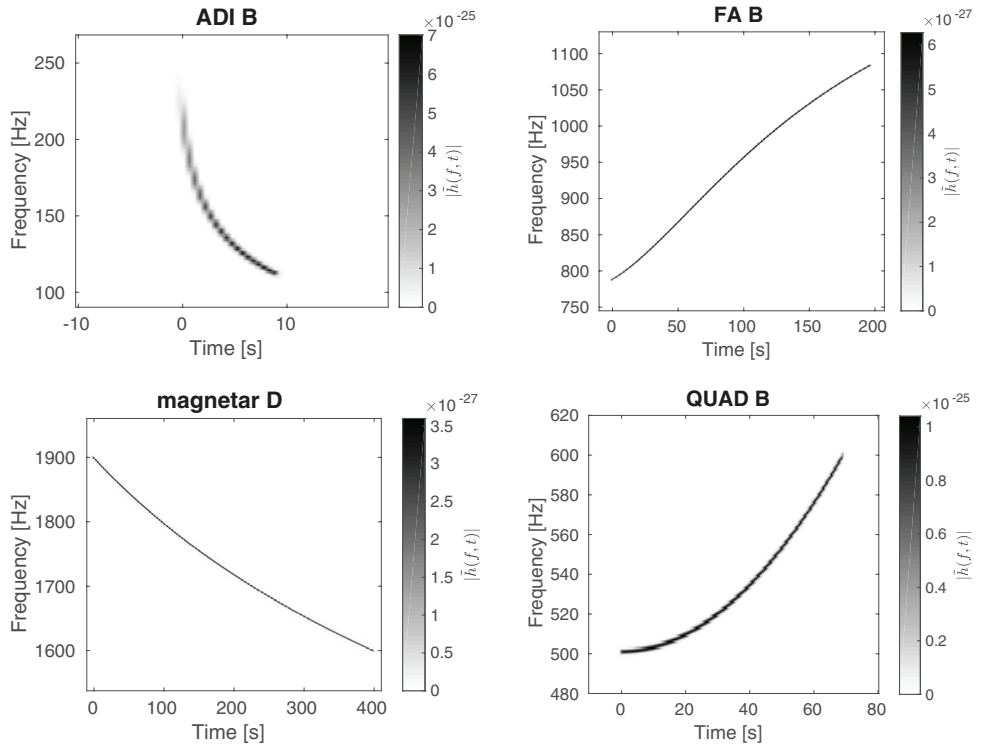

Figure 1. Time-frequency representation (1 s × 1 Hz resolution spectrogram) of some of the signal waveforms used to estimate the sensitivity of the searches.

also varied in order to estimate the dependency of the efficiency on the strength of the signal at a given FAR. Efficiency is simply the fraction of signals that are detected with a ranking statistic equal or larger than a value corresponding to the given FAR. To measure the intrinsic amplitude strength of a waveform, we use the root-sum-square strain amplitude at the Earth $h_{\rm rss}$ defined as in [27],

$$h_{\rm rss} = \sqrt{\int_{-\infty}^{\infty} (H_+^2(t) + H_\times^2(t))\,{\rm d}t}, \tag{2}$$

where H_+ and $H_\times$ are the GW strain polarizations in the source frame. Table 1 provides the values of $h_{\rm rss}$ at which each pipeline recovers 50% or fewer of the injected signals for a FAR of 1 event in 50 years. Generally, cWB, Zebragard and X-SphRad have similar sensitivities while Lonetrack is better by a factor 2 for the waveforms that are well fit by Bézier curves (LINE and QUAD).

Some of the listed waveforms are not detectable by a given pipeline. This is naturally the case for >1 kHz signals for X-SphRad. But this is also the case for monochromatic signals (MONO and SG) for cWB and Lonetrack. The reasons are different for each pipeline. For example, the way the pipelines whiten the data or estimate the detector noise power spectrum may wash out continuous signals. This is the case for cWB and to a lesser extent for Zebragard and X-SphRad. Lonetrack by construction has no sensitivity to monochromatic signals and band limited white noise as these types of waveforms are not modelled by a Bezier curve.

Table 1. Search sensitivity of the four pipelines to the 22 waveform families used to cover the unmodeled long transient parameter space. The h_{rss} at 50% efficiency is computed for a FAR of 1 event in 50 years. $E_{\rm GW}^{50\%}$ is the GW energy emitted by a source located at 10 kpc for which the search efficiency drops below 50% for a FAR of 1 event in 50 years. The models are not sequentially named to avoid confusion with models used in former studies. The second column provides the parameters of the waveforms as defined in section 3.1 or in [27].

	Properties			$h_{\rm rss}^{50\%}$ (1×10^{-21} Hz$^{1/2}$)				$E_{\rm GW}^{50\%}$ ($\mathrm{M}_\odot\mathrm{c}^2$)			
					STAMP-AS				STAMP-AS		
Waveform	Parameters	Duration (s)	Frequency (Hz)	cWB	Zebragard	Lonetrack	X-SphRad	cWB	Zebragard	Lonetrack	X-SphRad
FA A	—	25	1200–1500	2.55	2.05	1.62	—	1.32×10^{-05}	8.49×10^{-06}	5.36×10^{-06}	—
FA B	—	197	800–1075	2.19	2.02	1.16	—	4.77×10^{-06}	4.04×10^{-06}	1.34×10^{-06}	—
ADI A	$M = 5\ \mathrm{M}_\odot$ $a_* = 0.3$ $\epsilon = 0.05$	39	135–166	0.48	0.54	0.42	0.39	5.84×10^{-09}	7.32×10^{-09}	4.43×10^{-09}	3.83×10^{-09}
ADI B	$M = 10\ \mathrm{M}_\odot$ $a_* = 0.95$ $\epsilon = 0.2$	9	110–209	0.51	0.55	0.57	0.52	6.45×10^{-09}	7.35×10^{-09}	7.98×10^{-09}	7.43×10^{-09}
ADI C	$M = 10\ \mathrm{M}_\odot$ $a_* = 0.95$ $\epsilon = 0.04$	236	130–251	1.07	1.02	0.76	1.38	2.97×10^{-08}	2.71×10^{-08}	1.49×10^{-08}	4.91×10^{-08}
ADI D	$M = 3\ \mathrm{M}_\odot$ $a_* = 0.7$ $\epsilon = 0.035$	142	119–173	0.86	1.04	0.70	1.08	1.66×10^{-08}	2.45×10^{-08}	1.12×10^{-08}	2.65×10^{-08}
ADI E	$M = 8\ \mathrm{M}_\odot$ $a_* = 0.99$ $\epsilon = 0.065$	76	111–260	0.75	0.64	0.55	1.31	1.51×10^{-09}	1.11×10^{-09}	8.10×10^{-09}	4.68×10^{-08}
Magnetar D	$\epsilon_b = 0.005$ $f_0 = 1598$ Hz	400	1598–1900	5.07	6.72	3.70	—	4.62×10^{-05}	8.12×10^{-05}	2.49×10^{-05}	—
Magnetar E	$\epsilon_b = 0.01$ $f_0 = 1171$ Hz	400	1171–1450	3.99	3.94	2.11	—	2.14×10^{-05}	2.09×10^{-05}	5.97×10^{-06}	—

(*Continued*)

Table 1. (*Continued*)

	Properties			$h_{\rm rss}^{50\%}$ (1×10^{-21} Hz$^{1/2}$)				$E_{\rm GW}^{50\%}$ ($M_\odot c^2$)			
					STAMP-AS				STAMP-AS		
Waveform	Parameters	Duration (s)	Frequency (Hz)	cWB	Zebragard	Lonetrack	X-SphRad	cWB	Zebragard	Lonetrack	X-SphRad
Magnetar F	$\epsilon_b = 0.5$ $f_0 = 579$ Hz	400	579–950	2.46	2.09	1.18	1.75	3.40×10^{-06}	2.46×10^{-06}	7.79×10^{-07}	1.73×10^{-06}
Magnetar G	$\epsilon_b = 0.08$ $f_0 = 405$ Hz	400	400–490	1.72	2.14	1.22	1.04	6.40×10^{-07}	9.89×10^{-07}	3.18×10^{-07}	2.36×10^{-07}
MONO A	$f_0 = 90$ Hz $\frac{df}{dt} = 0$ $\frac{d^2f}{dt^2} = 0$	150	90	—	3.28	—	3.70	—	9.80×10^{-08}	—	1.24×10^{-07}
MONO C	$f_0 = 405$ Hz $\frac{df}{dt} = 0$ $\frac{d^2f}{dt^2} = 0$	250	405	—	2.92	—	3.28	—	1.52×10^{-06}	—	1.92×10^{-06}
LINE A	$f_0 = 50$ Hz $\frac{df}{dt} = 0.6$ Hz s^{-1} $\frac{d^2f}{dt^2} = 0$	250	50–200	1.12	1.25	0.64	3.01	2.45×10^{-08}	3.08×10^{-08}	8.05×10^{-09}	1.78×10^{-07}
LINE B	$f_0 = 900$ Hz $\frac{df}{dt} = -2$ Hz s^{-1} $\frac{d^2f}{dt^2} = 0$	100	700–900	1.62	1.28	0.76	1.60	1.67×10^{-06}	1.04×10^{-06}	3.62×10^{-07}	1.63×10^{-06}
QUAD A	$f_0 = 50$ Hz $\frac{df}{dt} = 0$ $\frac{d^2f}{dt^2} = 0.33$ Hz s^{-2}	30	50–200	0.83	0.75	0.66	1.81	9.02×10^{-09}	7.34×10^{-09}	5.72×10^{-09}	4.28×10^{-08}

(*Continued*)

Table 1. (*Continued*)

	Properties			$h_{\rm rss}^{50\%}$ (1×10^{-21} Hz$^{1/2}$)				$E_{\rm GW}^{50\%}$ ($M_\odot c^2$)			
					STAMP-AS				STAMP-AS		
Waveform	Parameters	Duration (s)	Frequency (Hz)	cWB	Zebragard	Lonetrack	X-SphRad	cWB	Zebragard	Lonetrack	X-SphRad
QUAD B	$f_0 = 500$ Hz $\frac{df}{dt} = 0$ $\frac{d^2f}{dt^2} = 0.04$ Hz s^{-2}	70	500–600	1.21	1.07	0.75	.96	4.43×10^{-07}	3.48×10^{-07}	1.69×10^{-07}	2.76×10^{-07}
SG A	$f_0 = 90$ Hz $\tau = 30$ s	150	90	—	5.50	—	3.42	—	2.84×10^{-07}	—	1.10×10^{-07}
SG C	$f_0 = 405$ Hz $\tau = 5050$ s	250	405	—	3.79	—	1.95	—	2.57×10^{-06}	—	6.81×10^{-07}
WNB A	—	20	50-400	2.86	2.04	—	4.74	5.17×10^{-07}	2.63×10^{-07}	—	1.42×10^{-06}
WNB B	—	60	300-350	2.93	1.97	—	1.73	1.80×10^{-06}	4.52×10^{-07}	—	3.49×10^{-07}
WNB C	—	100	700-750	5.36	3.20	—	—	1.53×10^{-05}	5.45×10^{-06}	—	—

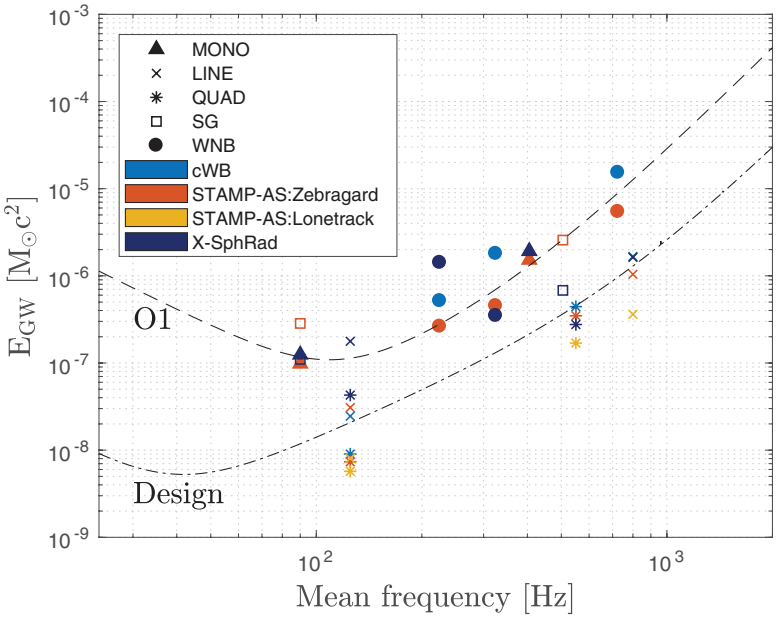

Figure 2. Emitted GW energy versus frequency for sources located at 10 kpc detected with 50% efficiency and a FAR of 1 event in 50 years. Results are shown for all the ad-hoc waveforms. The 'O1' and 'Design' curves are obtained with a monochromatic signal single template matched filtering search using the measured O1 and the predicted high-power signal recycling zero-detuning Advanced LIGO [49] sensitivity curves respectively. Both curves are rescaled so that the curve 'O1' matches the MONO results of this search. X-SphRad and cWB LINE B (∼800 Hz) results are overlapping.

Figure 2 displays the GW energy emitted by a source located at 10 kpc for which the search efficiency drops below 50% for a FAR of 1 event in 50 years. The energy provides a universal quantity that can be directly compared to astrophysical predictions of the different possible sources. Assuming an isotropic GW emission, the energy emitted by a source at a distance r is given by

$$E_{\rm GW} = \frac{c^3 r^2}{4G} \int_{-\infty}^{\infty} \langle \dot{h}_+^2 + \dot{h}_\times^2 \rangle \, {\rm d}t, \tag{3}$$

where $\dot{h}_+$ and $\dot{h}_\times$ are the time derivative of the GW strain for the two polarizations in the detector frame. For the sake of visibility, only ad-hoc model waveforms are considered in the figure while values for all waveforms are reported in table 1. It illustrates the dependence on the signal frequency which roughly follows the detectors' sensitivity. Yet, one also sees that monochromatic (MONO and SG) and band limited white noise (WNB) waveform detections are systematically less efficient than the other waveforms. The minimal GW energy emitted by a source detected in the Galaxy (10 kpc) is of the order of a few $10^{-8}\,{\rm M}_\odot{\rm c}^2$. If one now looks at each pipeline's performance, for a given type of source, the detectable GW energy is spread over almost one order of magnitude and the most sensitive pipeline is different for each source.

To project the search sensitivity forward to the Advanced LIGO detectors design sensitivity, we have considered the matched filtered search results for an idealized monochromatic signal with a detection SNR threshold of 8. We are using monochromatic signals because the

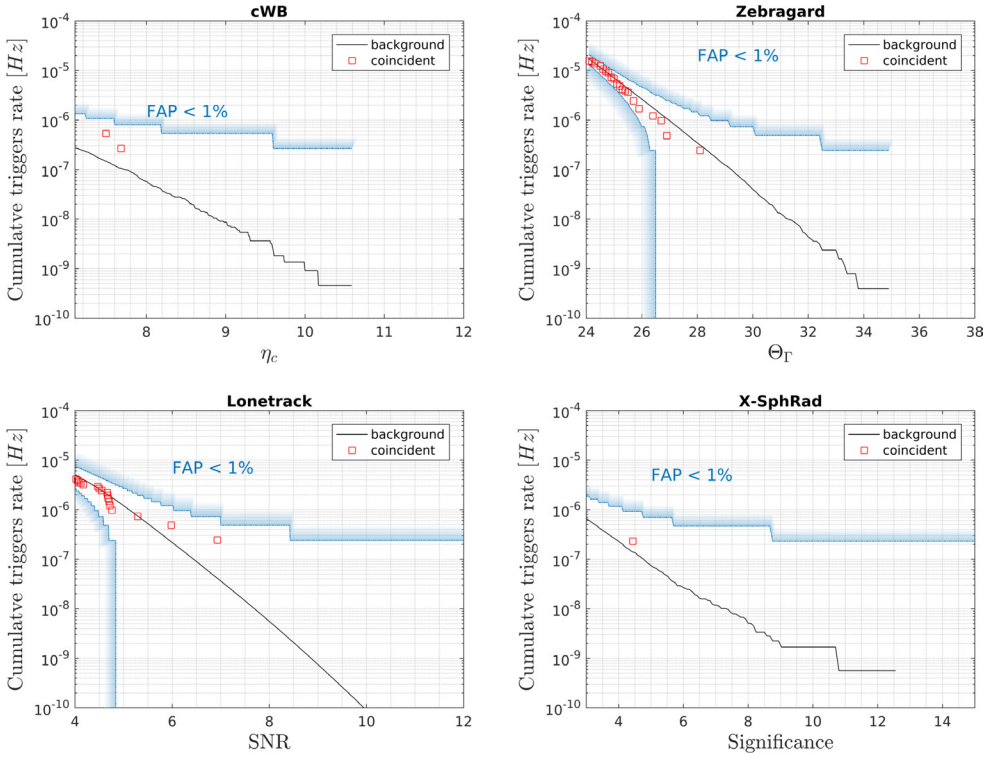

Figure 3. Cumulative trigger rate as function of the triggers' ranking statistic for the four pipelines. The coincident triggers are represented by the red squares while the black curves show the estimation of the contribution of the accidental coincident noise triggers. The blue isocurves indicate the trigger rate that corresponds to a false alarm probability (FAP) lower than 1%. This illustrates that all coincident triggers' distributions are compatible with the expected background. For cWB and X-SphRad the lower isocurve is not displayed because it falls outside of the axis limits.

frequency is well defined. Results are then rescaled with a single factor such that the 'O1' curve approximatively matches the MONO results of the O1 search. The 'Design' curve is obtained using the predicted design Advanced LIGO high-power signal recycling zero-detuning sensitivity curves [49], rescaled using the same factor as the 'O1' curve. These curves show how the sensitivity to monochromatic signals will evolve through the future observing runs assuming a FAR of 1 event in 50 years. In particular, a gain of two orders of magnitude on the energy is expected at low frequency with the Advanced LIGO design sensitivity. Similar trends for the other waveforms are expected.

5. Search results

Figure 3 shows the distributions of the cumulative rate of coincident data triggers for each pipeline; these are ranked according to the pipelines' detection statistic and are shown together with the estimated background. The X-SphRad and cWB distributions contain fewer triggers than the Zebragard or Lonetrack distributions because of the selection criteria that remove many low significant triggers at early stages. No significant excess of coincident triggers is found by any pipeline. The properties of the most significant triggers from each pipeline are

Table 2. Properties of the most significant coincident triggers found by each of the long transient search pipelines during the O1 observational run. FAP is the probability of observing at least 1 noise trigger more significant that the most significant coincident trigger.

Pipeline GPS time	Ranking statistic	FAP	Frequency (Hz)	Duration (s)
cWB 1132990790	$\eta_c = 7.6$	0.33	2039–2041	5.5
Zebragard 1131758576	$\Theta_\Gamma = 28.2$	0.72	1034–1120	51
Lonetrack 1136368706	SNR = 6.95	0.36	85–1549	208
X-SphRad 1135861536	Significance = 4.5	0.44	895–909	4

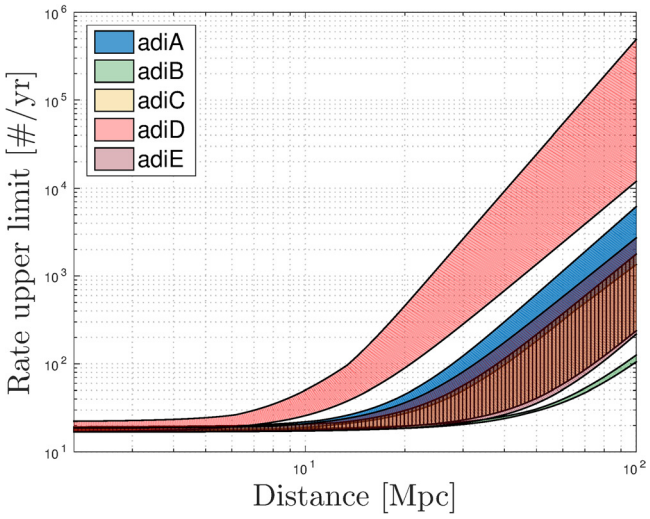

Figure 4. Upper limits at 90% confidence on the rate of GW events from accretion disk instability as a function of the distance. The band covers the results from the best and the worst pipelines for each tested waveforms. O1 amplitude calibration errors are accounted for in the upper limits calculation.

reported in table 2. They are all compatible with the O1 background expectations as underlined by the rather large values of their false alarm probabilities (FAP). The FAP is the probability of observing at least one background trigger with a ranking statistic larger than a given threshold.

Given the absence of long-duration transient GWs in the O1 data, we have updated the limits established in [27]. Assuming a Poissonian distribution of long-duration GW sources, we compute the 90% confidence level limit of the trigger rate using the loudest event statistic method [50], where systematic uncertainty coming from the strain amplitude calibration is folded into the upper limit calculation as in [27]. During the O1 science run, the amplitude calibration 99th percentile uncertainty was measured to be 6% and 17% for the H1 and L1 detectors, respectively, in the 24–2048 Hz frequency band [47].

Figure 4 shows the rate upper limit as a function of distance for the ADI signals. The area is defined by the most and the least performing pipelines. The exclusion rate at short distance is

Table 3. Distances at which the pipeline efficiency drops below 50% for a FAR of 1 event in 50 years for the accretion disk instability, magnetar and fallback accretion signals considered in the O1 search.

Waveform	Distance$^{50\%}$ (Mpc)			
		STAMP-AS		
	cWB	Zebragard	Lonetrack	X-SphRad
FA A	1.08	1.34	1.69	—
FA B	1.76	1.91	3.32	—
ADI A	19.1	17.1	22.0	23.6
ADI B	58.3	54.6	52.5	54.4
ADI C	29.1	30.5	41.1	22.6
ADI D	10.1	8.33	12.3	8.02
ADI E	33.6	39.2	46.0	19.1
Magnetar D	0.14	0.11	0.19	—
Magnetar E	0.20	0.20	0.37	—
Magnetar F	0.50	0.57	1.02	0.68
Magnetar G	0.43	0.35	0.61	0.71

limited by the observational duration. Since O1 is shorter than S5 or S6, the event rate is less constrained. Conversely, the maximal distance for which one can expect to detect an event is improved by a factor $\sim$3.

Distances at which we can detect a signal with 50% efficiency are compared for all astrophysical waveforms in table 3. As already seen, detection distances for the 5 ADI waveforms are between 10–60 Mpc. On the other hand, the chance of detecting GWs from a magnetar or from the accretion of a black hole is limited to sources in the local group.

The fact that we do not see any signals in O1 is not unexpected. First, O1 is a short run, with only 49 d of total coincident data, which is enough to detect multiple coalescences of binary black holes but quite short to detect long-duration GW signals considering the large uncertainties or unknowns about the rates of each of the potential long transient GW sources. Next, the energy of a long-duration signal is spread over a large number of pixels, which causes a decrease in the sensitivity of the pipelines. This explains why the short transient O1 search [12] is roughly an order of magnitude more sensitive at a given frequency. Nevertheless, when compared to the S5/S6 results [27], the O1 long-duration transient search is better by a factor $\sim$10 due to the improvements in detector sensitivities.

6. Conclusion

This paper reports the results of an all-sky search for unmodeled long-duration transient GWs in the first Advanced LIGO observing run. The parameter space covered by this search has been increased compared to the preceding search. Four different pipelines have searched for GW signals to efficiently cover the large space of possible waveforms. The most significant triggers found by each pipeline are consistent with the noise background, excluding for now a long duration GW transient detection.

Upper limits have been set on the rate of events for three families of long-duration GW transients (fallback accretion on neutron stars, black hole accretion disk instabilities and magnetar giant flares). They indicate we are sensitive to potential sources in the local group. Alternatively, if we consider a source in the Galaxy (10 kpc) we are sensitive to sources

emitting at least $6 \times 10^{-9}\ M_{\odot}c^2$ for frequencies where the detectors' sensitivities are maximal. This is a lower bound (our results are spread over almost two orders of magnitude) but this is still an interesting achievement as it addresses an energy range that is astrophysically relevant [51, 52]. New data have been acquired recently by the LIGO detectors (observing run O2) with a sensitivity similar to O1 and a longer observation time which increases the chance of observing a long-duration transient GW source [53]. The Advanced Virgo detector has joined for the first time the advanced GW detector network on 1 August 2017; this increases sky coverage and improves the prospects for detection. In a few years, Advanced LIGO and Advanced Virgo should reach their design sensitivities. We have shown that we should gain between one and two orders of magnitude, depending on the frequency range, in the sensitivity to detect GW energy as low as $\sim 10^{-8}\ M_{\odot}c^2$ for a source emitting a monochromatic signal at $\sim$90 Hz and located at 10 (kpc).

Acknowledgments

The authors gratefully acknowledge the support of the United States National Science Foundation (NSF) for the construction and operation of the LIGO Laboratory and Advanced LIGO as well as the Science and Technology Facilities Council (STFC) of the United Kingdom, the Max-Planck-Society (MPS), and the State of Niedersachsen/Germany for support of the construction of Advanced LIGO and construction and operation of the GEO600 detector. Additional support for Advanced LIGO was provided by the Australian Research Council. The authors gratefully acknowledge the Italian Istituto Nazionale di Fisica Nucleare (INFN), the French Centre National de la Recherche Scientifique (CNRS) and the Foundation for Fundamental Research on Matter supported by the Netherlands Organisation for Scientific Research, for the construction and operation of the Virgo detector and the creation and support of the EGO consortium. The authors also gratefully acknowledge research support from these agencies as well as by the Council of Scientific and Industrial Research of India, the Department of Science and Technology, India, the Science & Engineering Research Board (SERB), India, the Ministry of Human Resource Development, India, the Spanish Agencia Estatal de Investigación, the Vicepresidència i Conselleria d'Innovació, Recerca i Turisme and the Conselleria d'Educació i Universitat del Govern de les Illes Balears, the Conselleria d'Educació, Investigació, Cultura i Esport de la Generalitat Valenciana, the National Science Centre of Poland, the Swiss National Science Foundation (SNSF), the Russian Foundation for Basic Research, the Russian Science Foundation, the European Commission, the European Regional Development Funds (ERDF), the Royal Society, the Scottish Funding Council, the Scottish Universities Physics Alliance, the Hungarian Scientific Research Fund (OTKA), the Lyon Institute of Origins (LIO), the Paris Île-de-France Region, the National Research, Development and Innovation Office Hungary (NKFI), the National Research Foundation of Korea, Industry Canada and the Province of Ontario through the Ministry of Economic Development and Innovation, the Natural Science and Engineering Research Council Canada, the Canadian Institute for Advanced Research, the Brazilian Ministry of Science, Technology, Innovations, and Communications, the International Center for Theoretical Physics South American Institute for Fundamental Research (ICTP-SAIFR), the Research Grants Council of Hong Kong, the National Natural Science Foundation of China (NSFC), the Leverhulme Trust, the Research Corporation, the Ministry of Science and Technology (MOST), Taiwan and the Kavli Foundation. The authors gratefully acknowledge the support of the NSF, STFC, MPS, INFN, CNRS and the State of Niedersachsen/Germany for provision of computational resources.

References

[1] Abbott B P *et al* 2016 Observation of gravitational waves from a binary black hole merger *Phys. Rev. Lett.* **116** 061102
[2] Abbott B P *et al* 2016 GW151226: observation of gravitational waves from a 22-solar-mass binary black hole coalescence *Phys. Rev. Lett.* **116** 241103
[3] Abbott B P *et al* 2016 Binary black hole mergers in the first Advanced LIGO observing run *Phys. Rev.* X **6** 041015
[4] Abbott B P *et al* 2016 Observing gravitational-wave transient GW150914 with minimal assumptions *Phys. Rev.* D **93** 122004
[5] Abbott B P *et al* 2016 GW150914: first results from the search for binary black hole coalescence with Advanced LIGO *Phys. Rev.* D **93** 122003
[6] Abbott B P *et al* 2017 GW170104: observation of a 50-solar-mass binary black hole coalescence at redshift 0.2 *Phys. Rev. Lett.* **118** 221101
[7] Abbott B P *et al* 2017 GW170814: a three-detector observation of gravitational waves from a binary black hole coalescence *Phys. Rev. Lett.* **119** 141101
[8] Abbott B P *et al* 2017 GW170817: observation of gravitational waves from a binary neutron star inspiral *Phys. Rev. Lett.* **119** 161101
[9] Abbott B P *et al* 2017 Gravitational waves and gamma-rays from a binary neutron star merger: GW170817 and GRB 170817A *Astrophys. J.* **848** L13
[10] Abbott B P *et al* 2017 Multi-messenger observations of a binary neutron star merger *Astrophys. J.* **848** L12
[11] Abbott B P *et al* 2016 Upper limits on the rates of binary neutron star and neutron starblack hole mergers from advanced Ligos first observing run *Astrophys. J.* **832** L21
[12] Abbott B P *et al* 2017 All-sky search for short gravitational-wave bursts in the first Advanced LIGO run *Phys. Rev.* D **95** 042003
[13] Abbott B P *et al* 2017 Search for intermediate mass black hole binaries in the first observing run of Advanced LIGO *Phys. Rev.* D **96** 022001
[14] Lai D and Shapiro S L 1995 Gravitational radiation from rapidly rotating nascent neutron stars *Astrophys. J.* **442** 259
[15] Cutler C 2002 Gravitational waves from neutron stars with large toroidal B fields *Phys. Rev.* D **66** 084025
[16] Piro A L and Ott C D 2011 Supernova fallback onto magnetars and propeller-powered supernovae *Astrophys. J.* **736** 108
[17] Piro A L and Thrane E 2012 Gravitational waves from fallback accretion onto neutron stars *Astrophys. J.* **761** 63
[18] Piro A L and Pfahl E 2007 Fragmentation of collapsar disks and the production of gravitational waves *Astrophys. J.* **658** 1173
[19] van Putten M H P M 2001 Proposed source of gravitational radiation from a torus around a black hole *Phys. Rev. Lett* **87** 091101
[20] van Putten M H P M 2008 Gravitational waveforms of kerr black holes interacting with high-density matter *Astrophys. J. Lett.* **684** L91
[21] Corsi A and Mészáros P 2009 Gamma-ray burst afterglow plateaus and gravitational waves: multi-messenger signature of a millisecond magnetar? *Astrophys. J.* **702** 1171
[22] Gualtieri L, Ciolfi R and Ferrari V 2011 Structure, deformations and gravitational wave emission of magnetars *Class. Quantum Grav.* **28** 114014
[23] Metzger B D, Giannios D, Thompson T A, Bucciantini N and Quataert E 2011 The proto-magnetar model for gamma-ray bursts *Mon. Not. R. Astron. Soc.* **413** 2031
[24] Rowlinson A, O'Brien P T, Metzger B D, Tanvir N R and Levan A J 2013 Signatures of magnetar central engines in short GRB light curves *Mon. Not. R. Astron. Soc.* **430** 1061
[25] Marek A, Janka H T and Mueller E 2009 Equation-of-state dependent features in shock-oscillation modulated neutrino and gravitational-wave signals from supernovae *Astron. Astrophys.* **496** 475
[26] Murphy J W, Ott C D and Burrows A 2009 A Model for gravitational wave emission from neutrino-driven core-collapse supernovae *Astrophys. J.* **707** 1173–90
[27] Abbott B P *et al* 2016 All-sky search for long-duration gravitational wave transients with initial LIGO *Phys. Rev.* D **93** 042005
[28] Abbott B P *et al* 2016 Characterization of transient noise in Advanced LIGO relevant to gravitational wave signal GW150914 *Class. Quantum Grav.* **33** 134001

[29] Christensen N 2010 LIGO S6 detector characterization studies *Class. Quantum Grav.* **27** 194010
[30] Aasi J *et al* 2015 Characterization of the LIGO detectors during their sixth science run *Class. Quantum Grav.* **32** 115012
[31] Was M, Bizouard M-A, Brisson V, Cavalier F, Davier M, Hello P, Leroy N, Robinet F and Vavoulidis M 2010 On the background estimation by time slides in a network of gravitational wave detectors *Class. Quantum Grav.* **27** 015005
[32] Klimenko S *et al* 2016 Method for detection and reconstruction of gravitational wave transients with networks of advanced detectors *Phys. Rev.* D **93** 042004
[33] Prestegard T 2016 Unmodeled searches for long-lasting gravitational-wave signals with LIGO and studies of underground seismic noise for future gravitational-wave detectors *Thesis* University of Minnesota
[34] Isogai T, (The Ligo Scientific Collaboration and The Virgo Collaboration) 2010 Used percentage veto for ligo and virgo binary inspiral searches *J. Phys.: Conf. Ser.* **243** 012005
[35] Farin G 1996 *Curves and Surfaces for CAGD and Fourth Edition: a Practical Guide* (New York: Academic)
[36] Thrane E and Coughlin M 2013 Searching for gravitational-wave transients with a qualitative signal model: seedless clustering strategies *Phys. Rev.* D **88** 083010
[37] Thrane E and Coughlin M 2014 Seedless clustering in all-sky searches for gravitational-wave transients *Phys. Rev.* D **89** 063012
[38] Coughlin M, Meyers P, Kandhasamy S, Thrane E and Christensen N 2015 Prospects for searches for long-duration gravitational-waves without time slides *Phys. Rev.* D **92** 043007
[39] Thrane E and Coughlin M 2015 Detecting gravitation-wave transients at 5: a hierarchical approach *Phys. Rev. Lett.* **115** 181102
[40] Coughlin M, Thrane E and Christensen N 2014 Detecting compact binary coalescences with seedless clustering *Phys. Rev.* D **90** 083005
[41] Coughlin M, Meyers P, Thrane E, Luo J and Christensen N 2015 Detectability of eccentric compact binary coalescences with advanced gravitational-wave detectors *Phys. Rev.* D **91** 063004
[42] Cannon K C 2007 Efficient algorithm for computing the time-resolved full-sky cross power in an interferometer with omnidirectional elements *Phys. Rev.* D **75** 123003
[43] Edwards M 2013 On the search for intermediate duration gravitational waves using the spherical harmonic basis *Thesis* University of Cardiff
[44] Sutton P J *et al* 2010 X-pipeline: an analysis package for autonomous gravitational-wave burst searches *New J. Phys.* **12** 053034
[45] Was M, Sutton P J, Jones G and Leonor I 2012 Performance of an externally triggered gravitational-wave burst search *Phys. Rev.* D **86** 022003
[46] Edwards M and Sutton P J 2012 A new glitch-rejection algorithm forged in the spherical harmonic basis *J. Phys:. Conf. Ser.* **363** 012025
[47] Abbott B P *et al* 2017 Calibration of the Advanced LIGO detectors for the discovery of the binary black-hole merger GW150914 *Phys. Rev.* D **95** 062003
[48] Dall'Osso S, Giacomazzo B, Perna R and Stella L 2015 Gravitational waves from massive magnetars formed in binary neutron star mergers *Astrophys. J.* **798** 25
[49] Shoemaker D 2009 Advanced ligo anticipated sensitivity curves LIGO *Report No* T0900288 (https://dcc.ligo.org/LIGO-T0900288/public)
[50] Brady P R, Creighton J D and Wiseman A G 2004 Upper limits on gravitational-wave signals based on loudest events *Class. Quantum Grav.* **21** S1775–82
[51] Turolla R, Zane S and Watts A 2015 Magnetars: the physics behind observations. A review *Rep. Prog. Phys.* **78** 116901
[52] Mueller E, Rampp M, Buras R, Janka H-T and Shoemaker D H 2004 Towards gravitational wave signals from realistic core collapse supernova models *Astrophys. J.* **603** 221–30
[53] Aasi J *et al* 2016 Prospects for observing and localizing gravitational-wave transients with Advanced LIGO and Advanced Virgo *Living Rev. Relativ.* **19** 1